Mathematics

Research article

Stress boundary layers for the Giesekus fluid at the static contact line in extrudate swell

Jonathan D. Evans* **and Morgan L. Evans**

Department of Mathematical Sciences, University of Bath, Bath, BA2 7AY, UK

* **Correspondence:** Email: masjde@bath.ac.uk.

Abstract: We used the method of matched asymptotic expansions to examine the behavior of the Giesekus fluid near to the static contact line singularity in extrudate swell. This shear-thinning viscoelastic fluid had a solution structure in which the solvent stresses dominated the polymer stresses near to the singularity. As such, the stress singularity was Newtonian dominated, but required viscoelastic stress boundary layers to fully resolve the solution at both the die wall and free surface. The sizes and mechanism of the boundary layers at the two surfaces were different. We gave a similarity solution for the boundary layer at the die wall and derived the exact solution for the boundary layer at the free-surface. The local behavior for the shape of the free-surface was also derived, which we showed was primarily determined by the solvent stress. However, the angle of separation of the free surface was determined by the the global flow geometry. It was this which determined the stress singularity and then in turn the free-surface shape.

Keywords: extrudate swell; Giesekus viscoelastic fluid; contact line stress singularity; matched asymptotics
Mathematics Subject Classification: 76A10, 76M45

1. Introduction

The stress singularity at a static contact line is a longstanding challenge for models of viscoelastic liquids. This phenomenon occurs when a fluid interface separates from a solid surface, such as during polymer extrusion where the fluid exits a channel (in applications termed a die). This situation is particularly significant for viscoelastic liquids because the diameter of the emerging jet is often several times larger than the channel, leading to extrudate swell (histroically termed die-swell). A critical aspect is that the fluid flow traverses the contact line at the solid/air junction. The abrupt change in boundary conditions, from no-slip on the solid channel wall to no-shear on the free surface outside the die, creates a singularity in the fluid stress field when the angle of fluid separation is sufficiently large.

This stress singularity presents issues for Newtonian fluids [1–3], but is particularly problematic for viscoelastic fluids due to the profound effects of their memory properties on flow behavior [4, 5]. This situation should be contrasted with edge flow [6] or rivulet flow [7–9], where the fluid flow is parallel to the contact line.

Extrusion is important in the polymer processing industry, where it is used for the manufacturing of many plastic pipe and profile products [10, 11]. The polymers used typically possess a macromolecular structure with long chains of repeating units. They are processed in a molten state, exhibiting very high viscosity and shear-thinning behavior (due to the alignment and disentanglement of the polymer chains with increasing shear-rate). In addition, they display elasticity, which is responsible for effects such as stress relaxation and normal stress differences [12–14]. Normal stress differences contribute to flow instabilities [15–17] and extrudate swelling [18]. The latter phenomenon is particularly striking in polymers, where a significant increase in cross-sectional area occurs [4, 5, 19].

The extrudate swell problem is not only relevant for industrial applications but also serves as a crucial computational test for viscoelastic fluids with free surfaces. It is a benchmark problem in computational rheology [20]. During the transition from fully-developed flow within the die to plug flow outside, the fluid jet swells due to stress relaxation at the surface. The maximum cross-sectional area of the jet is usually reached a few die-diameters downstream from the die exit. The behaviors of polymeric and Newtonian jets differ significantly [19]. For polymer melts and solutions, which are highly viscous and involve moderate velocities, the flow is primarily in the Stokes regime rather than at high Reynolds numbers. Polymeric jets show a substantial increase in the swelling ratio, where the dimension of the extrudate is seen experimentally as two to three times that of the die [21–25]. This constrasts with Newtonian jets, where the swelling ratio is only 1.1 to 1.2 [26–30]. As the Reynolds number increases, the swelling ratio for polymeric jets also increases, while for Newtonian jets, it decreases, leading to contraction at Re > 16. Higher Reynolds numbers are achievable experimentally for Newtonian fluids compared to polymeric fluids, which are limited to moderate flow rates due to instability and melt fracture at high extrusion rates [17]. This confines polymeric fluid dynamics to a low Reynolds number regime, where the swelling ratio increases with flow rate, and inertia effects are negligible.

As the polymeric fluid exits the die, the polymer free surface is assumed to remain attached to the die exit. This forms a three-phase contact point/line among two immiscible fluids and a solid. The interface shape evolves from this tri-junction until, in the absence of streamwise normal stresses, the polymer reaches its final thickness. Analyzing and simulating flows involving such contact points or lines is challenging due to a singularity in the rate-of-deformation and stress tensors. This singularity results from the change in boundary conditions from no-slip along the die wall to no-shear on the polymer free surface. The trijunction is usually modeled as a sharp corner with a fixed or static contact point/line [31], contrasting with moving contact lines in liquid/fluid/solid systems. Such singularities raise questions about the well-posedness of the mathematical problem, troublesome even for Newtonian flows and particularly acute for viscoelastic fluids. The physics near a contact line remains unclear and has been studied from both molecular and continuum perspectives [32–36]. At the continuum level, the presence of a stress singularity at the contact line suggests a breakdown of the theory, leading some researchers to introduce slip along the die-wall boundary in this vicinity. This approach has been used in both Newtonian cases [32, 37–41] and polymer models [42]. The origin of such slip may be attributed to true slip at the molecular level or apparent slip on a macroscopic scale

due to microscopic phenomena [43], such as surface roughness or the presence of a lower viscosity gas in surface grooves. Introducing wall slip significantly alters the local stress behavior, making it difficult to determine behavior in the no-slip case, even when slip effects are minor. In the no-slip case, the stress singularity is physically acceptable if integrable, ensuring a finite total force on the solid upstream die wall.

Numerous constitutive equations have been developed to relate stress and strain rates in polymer flows [44]. The Giesekus model, is based on the concept of a deformation dependent tensorial mobility for the polymer molecules [45]. It enables a qualitative description of a number of well-known properties of viscoelastic fluids, namely shear thinning, nonzero second normal stress coefficient and stress overshoot in transient shear flows [44, 46, 47].

This study continues the investigation into the stress singularity at the separation point for the Giesekus viscoelastic fluid. Currently, little is known about the behavior of this model near such points, unlike Newtonian viscous fluids [48]. Understanding these singularities tests the well-posedness of the constitutive equations and can improve numerical scheme convergence, similar to the Newtonian case [1, 2]. Preliminary findings on this problem were presented in [49], where the stress singularity was identified. However, the approach relied on order-of-magnitude estimates along streamlines without detailed examination of their mathematical solutions. Here, we address this issue by providing boundary layer solutions and setting the results on a more rigorous footing through matched asymptotic analysis. The key to this approach is aligning the polymer extra-stress tensor along streamlines, which reformulates the constitutive equations along their characteristics and enables the correct stress information to be transmitted between the different asymptotic regions. The analysis is able to quantify the effect of the singularity on the free-surface for the Giesekus model, which has been a key unknown for viscoelastic liquids [5]. The approach extends the results of the simpler stick-slip problem [50] and the asymptotic structure parallels that of the simplified Phan-Thien-Tanner (sPTT) model in [51], although the details of the boundary layers are very different.

2. Problem formulation and governing equations

We present here the geometry, summarized in Figure 1, and the dimensionless governing equations. The dimensional model is given in [49]. The velocity, pressure and extra-stress fields satisfy the conservation equations

$$\nabla \cdot \mathbf{u} = 0, \qquad \mathbf{0} = -\nabla p + \nabla \cdot \mathbf{T}, \tag{2.1}$$

where the total extra-stress $\mathbf{T} = \beta \mathbf{T}^s + (1 - \beta)\mathbf{T}^p$ has a Newtonian solvent component $\mathbf{T}^s = 2\mathbf{D}$ and the polymer extra-stress satisfies the Giesekus constitutive equation

$$\mathbf{T}^p + \mathrm{Wi} \left(\overset{\triangledown}{\mathbf{T}^p} + \kappa(\mathbf{T}^p)^2 \right) = 2\mathbf{D}, \tag{2.2}$$

with the upper convected derivative of stress and the rate of strain terms being

$$\overset{\triangledown}{\mathbf{T}^p} = (\mathbf{u} \cdot \nabla)\mathbf{T}^p - (\nabla \mathbf{u})^T \mathbf{T}^p - T^p(\nabla \mathbf{u}), \qquad 2\mathbf{D} = \nabla \mathbf{u} + (\nabla \mathbf{u})^T. \tag{2.3}$$
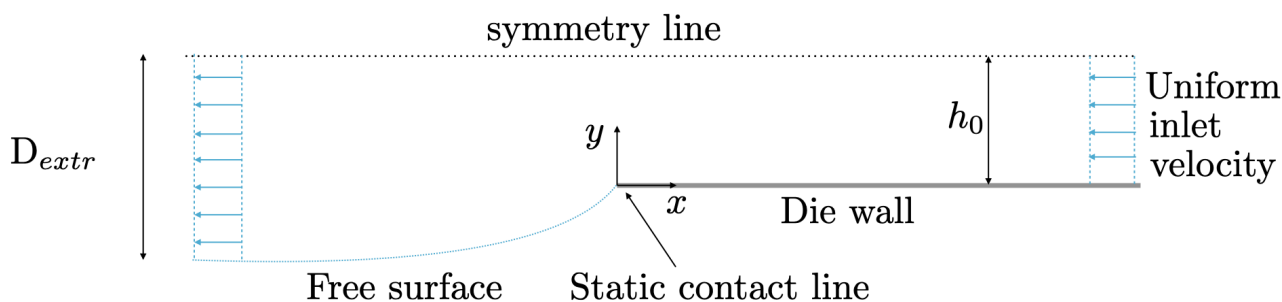
Figure 1. Schematic of the planar extrudate swell flow problem. The channel half-width is h_0 and the problem is symmetric about the mid-line $y = h_0$. Uniform flow enters at the inlet, transitioning to fully developed Poiseuille flow in the channel and eventually becoming plug flow of half-width D_{extr} on emergence from the channel.

The main dimensionless parameters are the Weissenberg number Wi ≥ 0, the solvent viscosity fraction $\beta \in [0, 1]$ and the mobility factor $\kappa \in [0, 1]$. Realistic behavior of the model is usually obtained for $0 < \kappa < 0.5$ [12, 52]. The analysis will be confined to the die exit, the local coordinate system for which at the lower die-wall is depicted in Figure 2. As boundary conditions, we have no-slip on the die-wall, whilst on the free-surface of the emerging jet we have the kinematic (or no-flux) condition, together with the tangential and normal stress balance presented as

$$\mathbf{u} \cdot \mathbf{n} = 0, \qquad \mathbf{m}^T \cdot \mathbf{T} \cdot \mathbf{n} = 0, \qquad \mathbf{n}^T \cdot \mathbf{T} \cdot \mathbf{n} = p - p_a + \frac{\mathcal{K}}{C_a}, \tag{2.4}$$

where C_a is the capillary number, p_a the external atmospheric pressure (taken as datum and thus set to zero), $\mathbf{m}$ unit tangent and $\mathbf{n}$ unit normal to the free surface.
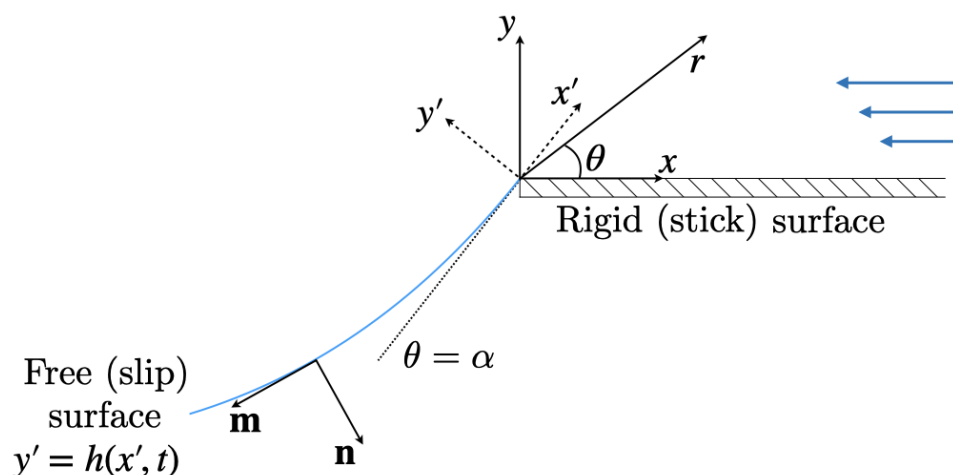

Figure 2. Local Cartesian and polar coordinates centered at the contact line singularity at the join of the lower wall and free surface.

The separation angle α is a parameter of the problem, its physical range of interest being between $\pi/2$ and $3\pi/2$. It is determined by the global flow rather than the normal stress condition in (2.4), which

specifies the free-surface curvature. The influence of surface tension is thus primarily on the shape of the free-surface and not the singularity, as explained in [53].

The formulation of the problem that we adopt is one where the velocity field (and an orthogonal vector) are used to span the polymer stress field. This idea was first suggested by Renardy [54, 55] as an approach to dealing with situations where the stress field encounters a geometrical singularity, such as at sharp corners. The mathematical basis for doing this, is that the polymer stress is then aligned with the streamlines of the flow, which are characteristics of the constitutive equations [56–58]. To achieve this, we write the polymer stress in the form

$$\mathbf{T}^p = \frac{1}{\mathrm{Wi}} \left(-\mathbf{I} + T_{uu}\mathbf{u}\mathbf{u}^T + T_{uw}(\mathbf{u}\mathbf{w}^T + \mathbf{w}\mathbf{u}^T) + T_{ww}\mathbf{w}\mathbf{w}^T \right), \tag{2.5}$$

where

$$\mathbf{u} = \begin{pmatrix} u \\ v \end{pmatrix}, \qquad \mathbf{w} = \frac{1}{\|\mathbf{u}\|^2} \begin{pmatrix} -v \\ u \end{pmatrix}, \tag{2.6}$$

and T_{uu}, T_{uw}, T_{ww} are the natural stress components. The component form of the Giesekus constitutive equation then gives the natural stress equations

$$T_{uu} + \mathrm{Wi}[(\mathbf{u} \cdot \nabla)T_{uu} + 2T_{uw}(\nabla \cdot \mathbf{w})] + \kappa \left(\frac{T_{uw}^2}{\|\mathbf{u}\|^2} + \left(T_{uu}\|\mathbf{u}\| - \frac{1}{\|\mathbf{u}\|} \right)^2 \right) = \frac{1}{\|\mathbf{u}\|^2},$$

$$T_{uw} + \mathrm{Wi}[(\mathbf{u} \cdot \nabla)T_{uw} + T_{ww}(\nabla \cdot \mathbf{w})] + \kappa \left(T_{uu}\|\mathbf{u}\|^2 - 2 + \frac{T_{ww}}{\|\mathbf{u}\|^2} \right) T_{uw} = 0, \tag{2.7}$$

$$T_{ww} + \mathrm{Wi}(\mathbf{u} \cdot \nabla)T_{ww} + \kappa \left(T_{uw}^2\|\mathbf{u}\|^2 + \left(\frac{T_{ww}}{\|\mathbf{u}\|} - \|\mathbf{u}\| \right)^2 \right) = \|\mathbf{u}\|^2.$$

These equations are in their steady form, which is the regime we investigate for the asymptotics. The unsteady version is required for full numerical simulations that we present in Section 4, a version of which can be found in [59].

3. Matched asymptotics

The goal is to determine the asymptotic behavior of the velocity and stress variables as the radial distance to the contact line vanishes. This asymptotic limit is inherently nonuniform and requires consideration of a three-region structure, summarized in Figure 3. It comprises narrow stress boundary layers for the polymer at both the die wall and free-surface linked through an outer (also termed core) region in which the solvent stress dominates. We approach the problem using the method of matched asymptotic expansions, with emphasis on deriving systematically the boundary layer equations and providing their solutions. We pose the problem in the sector $0 < r < \infty, 0 < \theta < \alpha$, with $\alpha \in [\pi/2, 3\pi/2]$. In this geometry, the problem is self-similar with no inherent length scale, so that we may take $\mathrm{Wi} = 1$ without loss of generality. The asymptotic results we derive will hold for any positive value of the Weissenberg number. However the Weissenberg number will influence the length scale on which the asymptotics dominate and we discuss this further in Section 5 using the numerical results in Section 4.
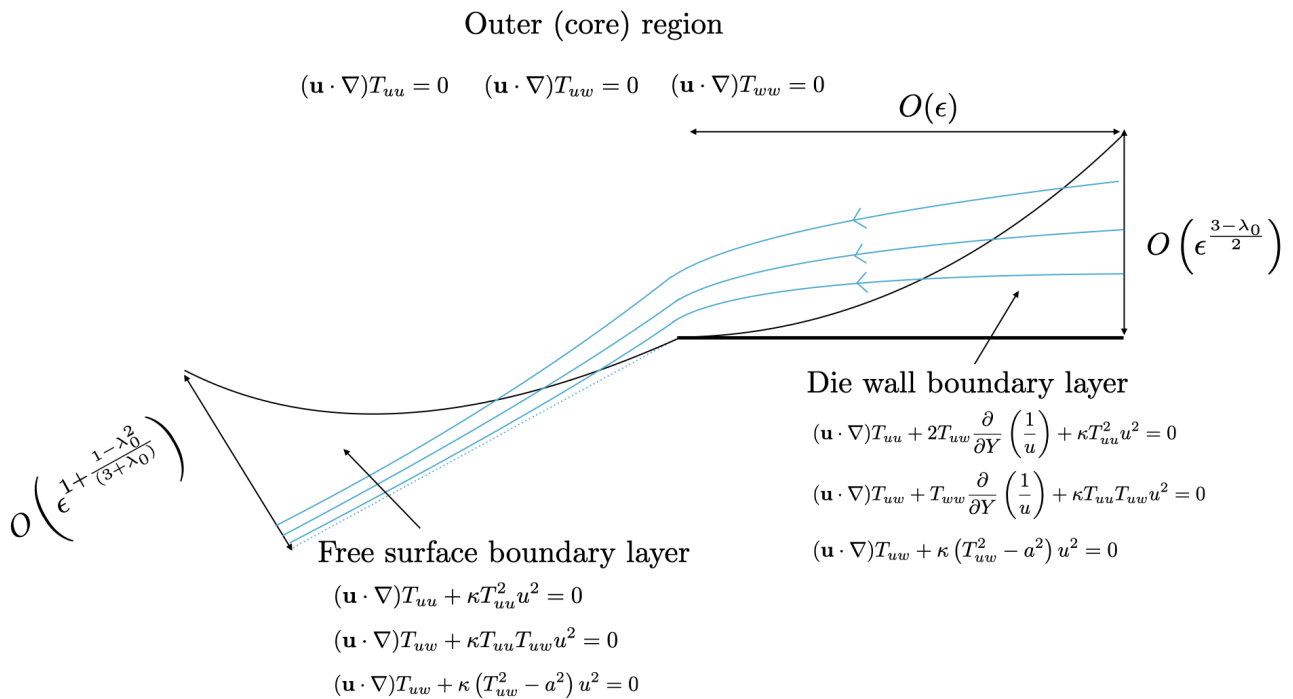
Outer (core) region

$$(\mathbf{u} \cdot \nabla) T_{uu} = 0 \qquad (\mathbf{u} \cdot \nabla) T_{uw} = 0 \qquad (\mathbf{u} \cdot \nabla) T_{ww} = 0$$

$O(\epsilon)$

$O\left(\epsilon^{\frac{3-\lambda_0}{2}}\right)$

Die wall boundary layer

$$(\mathbf{u} \cdot \nabla) T_{uu} + 2 T_{uw} \frac{\partial}{\partial Y}\left(\frac{1}{u}\right) + \kappa T_{uu}^2 u^2 = 0$$

$$(\mathbf{u} \cdot \nabla) T_{uw} + T_{ww} \frac{\partial}{\partial Y}\left(\frac{1}{u}\right) + \kappa T_{uu} T_{uw} u^2 = 0$$

$$(\mathbf{u} \cdot \nabla) T_{uw} + \kappa \left(T_{uw}^2 - a^2\right) u^2 = 0$$

$O\left(\epsilon^{1 + \frac{1 - \lambda_0^2}{(3 + \lambda_0)}}\right)$

Free surface boundary layer

$$(\mathbf{u} \cdot \nabla) T_{uu} + \kappa T_{uu}^2 u^2 = 0$$

$$(\mathbf{u} \cdot \nabla) T_{uw} + \kappa T_{uu} T_{uw} u^2 = 0$$

$$(\mathbf{u} \cdot \nabla) T_{uw} + \kappa \left(T_{uw}^2 - a^2\right) u^2 = 0$$

Figure 3. A schematic illustration of the asymptotic regions local to the static contact line singularity for the polymer stresses. Thin cusp-like boundary layers are located at each of the surfaces, whose thicknesses are different and depend on the separation angle through the eigenvalue λ_0. The outer (core) region holds away from the surfaces, the flow through which links the two boundary layers. The leading order polymer stress equations are summarized in each region.

3.1. The outer or core solution

The outer region is near to the separation point at the die exit, but still away from both the solid and free surfaces. The main behavior that identifies it, is that the solvent stress dominates the polymeric stress in this region, so that

$$1 \ll (1 - \beta) \mathbf{T}^p \ll \beta \mathbf{T}^s \qquad \text{as } r \to 0, \tag{3.1}$$

with both possessing singular behavior. In fact, Renardy [60] argues that this will be the case for most flows of interest where the Weissenberg number is large. Here the presence of the stress singularity, means that the "local" Weissenberg number is infinite, taken as the product of the shear rate (which goes infinite at the singularity) and the relaxation time. Thus many of the features of high Weissenberg number flows will manifest themselves in this problem, despite the actual Weissenberg number being unity, purely because of the singularity. In addition to (3.1), a further example will be the presence of the wall boundary layer being the same equations as those found for high Weissenberg numbers [61].

We now summarize the main results for this region from [49]. This gives the outer region a Newtonian balance $\mathbf{T} \sim \beta \mathbf{T}^s$ for the stress, and the momentum equation reduces to Stokes flow,

$$\mathbf{0} = -\nabla p + \beta \nabla^2 \mathbf{u}, \tag{3.2}$$

for which there are well-known separable solutions [48]. Using a stream function, these may be written as

$$\psi \sim \kappa C_0 r^{\lambda_0+1} f_0(\theta), \qquad p \sim 2\beta\kappa C_0 r^{\lambda_0-1} g_0(\theta) \qquad \text{as } r \to 0 \tag{3.3}$$

where C_0 is an arbitrary constant and expressions for the angular functions $f_0(\theta)$ and $g_0(\theta)$ can be found in [49] or [51].

The leading eigenvalue λ_0 depends on the separation angle α, and satisfies the transcendental equation

$$\lambda_0 \sin(2\alpha) = \sin(2\lambda_0\alpha). \tag{3.4}$$

A discussion on its behavior and the key angles is given in [53]. The stress singularity at the separation point is present for separation angles between 129° and 270°, with the swelling range greater than 180° being of relevance for viscoelastic fluids.

This Newtonian flow field in the core region gives order of magnitude estimates as

$$\mathbf{u} = O(r^{\lambda_0}), \quad \nabla\mathbf{u} = O(r^{\lambda_0-1}), \quad \mathbf{T}^s = O(r^{\lambda_0-1}) \qquad \text{as } r \to 0. \tag{3.5}$$

Using these orders of magnitude along with the assumption in (3.1) implies the dominance of the upper convected derivative in the polymeric stress equation resulting in

$$\overset{\triangledown}{\mathbf{T}^p} = 0. \tag{3.6}$$

The natural stress equations at leading order reduce to

$$(\mathbf{u} \cdot \nabla)T_{uu} = 0 \qquad (\mathbf{u} \cdot \nabla)T_{uw} = 0 \qquad (\mathbf{u} \cdot \nabla)T_{ww} = 0, \tag{3.7}$$

provided

$$\frac{T_{ww}}{\|\mathbf{u}\|^2} \ll T_{uw} \ll \|\mathbf{u}\|^2 T_{uu}, \tag{3.8}$$

which can be subsequently verified. At leading order, the natural stress variables are constant along streamlines, so that the asymptotic solution for the polymer stress in this region is

$$\mathbf{T}^p \sim T_{uu}(\psi)\mathbf{u}\mathbf{u}^T + T_{uw}(\psi)(\mathbf{u}\mathbf{w}^T + \mathbf{w}\mathbf{u}^T) - \mathbf{I} + T_{ww}(\psi)\mathbf{w}\mathbf{w}^T. \tag{3.9}$$

The first term is the well-known stretching solution and is an exact solution to (3.6). For convenience, power law forms are adopted for the stream function behavior of the natural stress variables,

$$T_{uu}(\psi) = \frac{C_1}{\kappa^2 C_0^2}\left(\frac{\psi}{\kappa C_0}\right)^{n_1}, \quad T_{uw} = C_2\left(\frac{\psi}{\kappa C_0}\right)^{n_2}, \quad T_{ww} = \kappa^2 C_0^2 C_3\left(\frac{\psi}{\kappa C_0}\right)^{n_3}, \tag{3.10}$$

where C_1, C_2, C_3 are arbitrary constants and the exponents

$$n_1 = -\frac{(\lambda_0 + 3)}{4}, \qquad n_2 = 0 \qquad n_3 = \frac{(\lambda_0 + 3)}{4}, \tag{3.11}$$

are determined by matching to the boundary layer behavior at the die wall (considered next). Initially, these exponents have to be carried through the analysis, but will be assumed known here for conciseness of exposition. Consequently, the singularity of the polymer stress is determined as

$$\mathbf{T}^p = O(r^{-\frac{(1-\lambda_0)(3-\lambda_0)}{4}}) \qquad \text{as } r \to 0^+, \tag{3.12}$$

which is subdominant to the solvent stress in (3.5), for all separation angles of interest (i.e., $1/3 < \lambda_0 < 1$). The required assumptions (3.1) and (3.8) can now be verified to hold for this asymptotic behavior. We remark that the presence of the solvent viscosity $\beta > 0$ is needed for this behavior, which no longer holds when β vanishes.

The behavior in (3.9) is not uniformly valid around the corner, but rather breaks down near the die wall and free surface. The reasons are different for the two locations. In the die wall case, the omission in (3.6) of the quadratic stress and rate-of-strain terms prevents the recovery of the necessary viscometric stress behavior associated with shear flow at the die wall. For the free-surface, it is only the quadratic stress terms that are required.

Using local Cartesian coordinates $x \sim r, y \sim r\theta$ as shown in Figure 2, we have the limiting behavior

$$\text{as } y \to 0^+, \; x > 0, \quad \psi \sim \kappa C_0 x^{\lambda_0-1} y^2, \; p \sim 2\beta\kappa g_0(0) C_0 x^{\lambda_0-1}, \; T_{uu} \sim \frac{C_1}{\kappa^2 C_0^2} x^{n_1(\lambda_0-1)} y^{2n_1},$$
$$T_{uw} \sim C_2, \quad T_{ww} \sim \kappa^2 C_0^2 C_3 x^{n_3(\lambda_0-1)} y^{2n_3}. \tag{3.13}$$

At the free-surface, using Cartesian coordinates $x' \sim -r, y' \sim r(\alpha - \theta)$ as orientated in Figure 2, we have the limiting behaviors

$$\text{as } y' \to 0^+, \; x' < 0, \quad \psi \sim \kappa C_0 C_\alpha (-x')^{\lambda_0} y', \; p \sim 2\beta\kappa C_0 g_0(\alpha)(-x')^{\lambda_0-1},$$
$$T_{uu} \sim \frac{C_1}{\kappa^2 C_0^2} C_\alpha^{n_1} (-x')^{\lambda_0 n_1} (y')^{n_1}, \quad T_{uw} \sim C_2, \tag{3.14}$$
$$T_{ww} \sim \kappa^2 C_0^2 C_3 C_\alpha^{n_3} (-x')^{\lambda_0 n_3} (y')^{n_3},$$

where the constant

$$C_\alpha = -f_0'(\alpha) = -\sin(\lambda_0 \alpha)/\lambda_0 \cos(\alpha) \tag{3.15}$$

is positive for all angles of interest. Although the natural stress T_{uu} is unbounded at the free-surface, this also translates into the leading-order Cartesian normal stress $T_{11}^p = T_{uu} u^2$ being unbounded. A narrow region at the free-surface, a stress boundary layer, is thus needed to arrest its growth. We note that the leading order polymer shear stress $T_{12}^p = T_{uu} uv$ does vanish at the free-surface.

3.2. The stress boundary layer at the die wall

An inner region is now sought at the die wall. To compare terms systematically, we introduce an artificial small parameter $\epsilon > 0$ through the scaling

$$x = \epsilon \bar{X}, \tag{3.16}$$

and consider $\bar{X} = O(1)$. The equations below are derived for the asymptotic limit $\epsilon \to 0$ and formal expansions are unnecessary since we deal with the leading order terms only. The introduction of this parameter allows us to perform a coordinate expansion of our system of equations in the neighborhood of the wall near to the singularity. Since the parameter ϵ is not present in the original system, it scales from the solution we derive. Physically it represents the length scale on which the small ϵ asymptotic behavior near to the singularity emerges. Estimates for it can be determined from numerical solution of the full problem presented in Section 4 and we discuss this in Section 5. The distinction between

coordinate and parameter expansions goes back to [62, 63], and the use of an artificial parameter is mentioned in the classic texts of [64–66].

The limiting behaviors in (3.13) and dominant balance in the polymer stress equations (2.7), when taken together determine the following scalings

$$y = \epsilon^{\frac{3-\lambda_0}{2}} \bar{Y}, \qquad \psi = \epsilon^2 \bar{\Psi}, \qquad u = \epsilon^{\frac{\lambda_0+1}{2}} \bar{u}, \qquad v = \epsilon \bar{v},$$
$$p = \epsilon^{\lambda_0-1} \bar{p}, \qquad T_{uu} = \epsilon^{-\frac{\lambda_0+3}{2}} \bar{T}_{uu}, \qquad T_{uw} = \bar{T}_{uw}, \qquad T_{ww} = \epsilon^{\frac{\lambda_0+3}{2}} \bar{T}_{ww}, \tag{3.17}$$

where the boundary layer variables are denoted by bars. The Cartesian components of the solvent stresses follow from the stream function as

$$T_{11}^s = \epsilon^{\frac{(\lambda_0-1)}{2}} \bar{T}_{11}^s \qquad T_{12}^s = \epsilon^{\lambda_0-1} \bar{T}_{12}^s \qquad T_{22}^s = \epsilon^{\frac{(\lambda_0-1)}{2}} \bar{T}_{22}^s, \tag{3.18}$$

where

$$\bar{T}_{11}^s = -\bar{T}_{22}^s = 2\frac{\partial^2 \bar{\Psi}}{\partial \bar{X} \partial \bar{Y}} \qquad \bar{T}_{12}^s = \frac{\partial^2 \bar{\Psi}}{\partial \bar{Y}^2}. \tag{3.19}$$

The scalings for the Cartesian components of the polymer extra-stresses may be determined from (2.5) as

$$T_{11}^p = \epsilon^{\frac{(\lambda_0-1)}{2}} \bar{T}_{11}^p, \qquad T_{12}^p = \bar{T}_{12}^p, \qquad T_{22}^p = -1 + \epsilon^{\frac{(1-\lambda_0)}{2}} \bar{T}_{22}^p, \tag{3.20}$$

where

$$\bar{T}_{11}^p = \bar{T}_{uu} \bar{u}^2, \quad \bar{T}_{12}^p = \bar{T}_{uu} \bar{u} \bar{v} + \bar{T}_{uw}, \quad \bar{T}_{22}^p = \bar{T}_{uu} \bar{v}^2 + 2\bar{T}_{uw} \frac{\bar{v}}{\bar{u}} + \frac{\bar{T}_{ww}}{\bar{u}^2}, \tag{3.21}$$

at leading order in ϵ. In the scalings of the total extra-stress components, the normal 11 component of the solvent and polymer stresses are comparable in this boundary layer, whilst the remaining polymer components remain subdominant to their solvent counterparts. The momentum equation for this inner region, $\bar{X} = O(1)$ and $\bar{Y} = O(1)$, reduces to

$$\frac{\partial^3 \bar{\Psi}}{\partial \bar{Y}^3} = 0, \qquad 0 = -\frac{\partial \bar{p}}{\partial \bar{Y}}, \tag{3.22}$$

at leading order. These imply that the stream function, solvent stresses and pressure remain unchanged at this order through this boundary layer with the explicit solution

$$\bar{\Psi} = \kappa C_0 \bar{X}^{\lambda_0-1} \bar{Y}^2, \qquad \bar{T}_{11}^s = -\bar{T}_{22}^s = 4(\lambda_0 - 1)\kappa C_0 \bar{X}^{\lambda_0-2} \bar{Y}, \qquad \bar{T}_{12}^s = 2\kappa C_0 \bar{X}^{\lambda_0-1}, \tag{3.23}$$

after matching to (3.13), which also givens the form of the pressure.

The leading order boundary layer equations for the polymer natural stresses are

$$(\bar{\mathbf{u}} \cdot \bar{\nabla}) \bar{T}_{uu} - 2\frac{\bar{T}_{uw}}{\bar{u}^2} \frac{\partial \bar{u}}{\partial \bar{Y}} + \kappa \bar{T}_{uu}^2 \bar{u}^2 = 0, \tag{3.24}$$

$$(\bar{\mathbf{u}} \cdot \bar{\nabla}) \bar{T}_{uw} - \frac{\bar{T}_{ww}}{\bar{u}^2} \frac{\partial \bar{u}}{\partial \bar{Y}} + \kappa \bar{T}_{uu} \bar{T}_{uw} \bar{u}^2 = 0, \tag{3.25}$$

$$(\bar{\mathbf{u}} \cdot \bar{\nabla}) \bar{T}_{ww} + \kappa \bar{u}^2 (\bar{T}_{uw}^2 - a^2) = 0, \tag{3.26}$$

with the parameter

$$a = \left(\frac{1 - \kappa}{\kappa} \right)^{\frac{1}{2}}. \tag{3.27}$$

We note that these are the same wall boundary layer equations obtained in the high Weissenberg limit [61], and, is a consequence of the singularity inducing high Weissenberg behavior locally in the fluid. We complete their statement, with viscometric stress behavior at the die wall

$$\text{as } \bar{Y} \to 0^+, \qquad \bar{T}_{uu} \sim \frac{a^{\frac{1}{2}}}{2\kappa^2}|C_0|^{-\frac{3}{2}}\bar{X}^{\frac{3(1-\lambda_0)}{2}}\bar{Y}^{-2},$$

$$\bar{T}_{uw} \sim aC_0|C_0|^{-1}, \tag{3.28}$$

$$\bar{T}_{ww} \sim 4a^{\frac{3}{2}}\kappa^2|C_0|^{\frac{3}{2}}\bar{X}^{\frac{3(\lambda_0-1)}{2}}\bar{Y}^2,$$

and outer matching conditions

$$\bar{Y} \to +\infty, \qquad \bar{T}_{uu} \sim \frac{C_1}{\kappa^2 C_0^2}\bar{X}^{\frac{(\lambda+3)(1-\lambda_0)}{4}}\bar{Y}^{-\frac{\lambda_0+3}{2}},$$

$$\bar{T}_{uw} \sim C_2, \tag{3.29}$$

$$\bar{T}_{ww} \sim \kappa^2 C_0^2 C_3 \bar{X}^{\frac{(\lambda_0+3)(\lambda_0-1)}{4}}\bar{Y}^{\frac{\lambda_0+3}{4}}.$$

We remark that the viscometric wall behavior (3.28) can be written in the more familiar Cartesian stress components using the component form of (2.5), which gives

$$\bar{T}_{11}^p \sim 2a^{\frac{1}{2}}|C_0|^{\frac{1}{2}}\bar{X}^{\frac{\lambda_0-1}{2}}, \qquad \bar{T}_{12}^p \sim aC_0|C_0|^{-1}, \qquad \bar{T}_{22}^p \sim a^{\frac{3}{2}}|C_0|^{-\frac{1}{2}}\bar{X}^{\frac{1-\lambda_0}{2}}. \tag{3.30}$$

Introducing the shear rate $\dot{\gamma} = \partial\bar{u}/\partial\bar{Y} = 2\kappa C_0\bar{X}^{\lambda_0-1}$, we have

$$T_{11}^p = \left(\frac{2a|C_0|\dot{\gamma}}{\kappa C_0}\right)^{\frac{1}{2}}, \qquad T_{12}^p = a\frac{C_0}{|C_0|}, \qquad T_{22}^p = -1 + \left(\frac{2a^3\kappa C_0}{\dot{\gamma}|C_0|}\right)^{\frac{1}{2}},$$

on the wall, which is the high shear rate viscometric behavior appropriate for the Giesekus model [61].

The governing equations (3.24)–(3.26), together with (3.28) and (3.29) possess a similarity solution in the form

$$\xi = a^{-\frac{1}{2}}|C_0|^{\frac{1}{2}}\frac{\bar{Y}}{\bar{X}^{\frac{3-\lambda_0}{2}}},$$

$$\bar{T}_{uu} = \frac{|C_0|^{-\frac{1}{2}}}{a^{\frac{1}{2}}\kappa^2}\bar{X}^{-\frac{\lambda_0+3}{2}}t_{uu}(\xi), \qquad \bar{T}_{uw} = at_{uw}(\xi) \qquad \bar{T}_{ww} = a^{\frac{5}{2}}\kappa^2|C_0|^{\frac{1}{2}}\bar{X}^{\frac{\lambda_0+3}{2}}t_{ww}(\xi),$$

the resultant set of ODEs being

$$2\xi^4\frac{dt_{uu}}{d\xi} + (\lambda_0+3)\xi^3 t_{uu} + t_{uw} \pm 4\xi^4 t_{uu}^2 = 0 \tag{3.31}$$

$$2\xi^4\frac{dt_{uw}}{d\xi} + \frac{t_{ww}}{2} \pm 4\xi^4 t_{uu}t_{uw} = 0 \tag{3.32}$$

$$2\xi^4\frac{dt_{ww}}{d\xi} - (\lambda_0+3)\xi^3 t_{ww} \pm 4\xi^4(t_{uw}^2-1) = 0 \tag{3.33}$$

with

$$\text{as } \xi \to 0^+, \quad t_{uu} \sim \frac{1}{2\xi^2}, \quad t_{uw} \sim \mp 1, \quad t_{ww} \sim 4\xi^2, \tag{3.34}$$

$$\text{as } \xi \to +\infty, \quad t_{uu} \sim C_1^* \xi^{-\frac{(\lambda_0+3)}{2}}, \quad t_{uw} \sim C_2^*, \quad t_{ww} \sim C_3^* \xi^{\frac{(\lambda_0+3)}{2}}, \tag{3.35}$$

and the scaled far-field constants

$$C_1^* = C_1 |C_0|^{\frac{\lambda_0-3}{4}} a^{-\frac{\lambda_0+1}{4}} \qquad C_2^* = \frac{C_2}{a} \qquad C_3^* = C_3 |C_0|^{\frac{3-\lambda_0}{4}} a^{\frac{\lambda_0-7}{4}}, \tag{3.36}$$

are introduced for convenience. The choice of upper sign in (3.31)–(3.35) occurs for the case $C_0 < 0$ corresponding to flow toward the singularity and is relevant to the extrudate swell situation. For completeness, the lower sign choice corresponds to the case $C_0 > 0$ and flow away from the singularity, which we simply record and don't pursue further here, as it would correspond to the reverse situation of the fluid entering the channel.

The nonlinear third-order system of Eqs (3.31)–(3.33) can be solved as an initial value problem with (3.34) posed as initial data and (3.35) to be determined. As implementation, we used MATLAB solver ode15s on the interval $[\xi_0, \xi_\infty]$ with $\xi_0 = 10^{-6}$ and $\xi_\infty \geq 10^{10}$ being sufficiently large to ensure convergence to (3.35). Figure 4 presents scaled profiles for $\alpha = 7\pi/6 \approx 210^o$, which we take as a representative case. The variation of the far-field constants with selected separation angles are given in Table 1.

Table 1. Numerical estimates of the far-field similarity parameters in (3.35) for given separation angles.

α (deg)	λ_0	C_1^*	C_2^*	C_3^*
130				
135	0.909	0.463	-0.931	4.031
150	0.731	0.401	-0.808	4.125
165	0.598	0.361	-0.725	4.231
180	0.500	0.334	-0.668	4.334
195	0.430	0.316	-0.629	4.423
210	0.383	0.304	-0.603	4.491
225	0.353	0.297	-0.588	4.535
240	0.339	0.293	-0.581	4.559
255	0.334	0.292	-0.578	4.568
270	0.333	0.292	-0.578	4.569

(a)

(b)
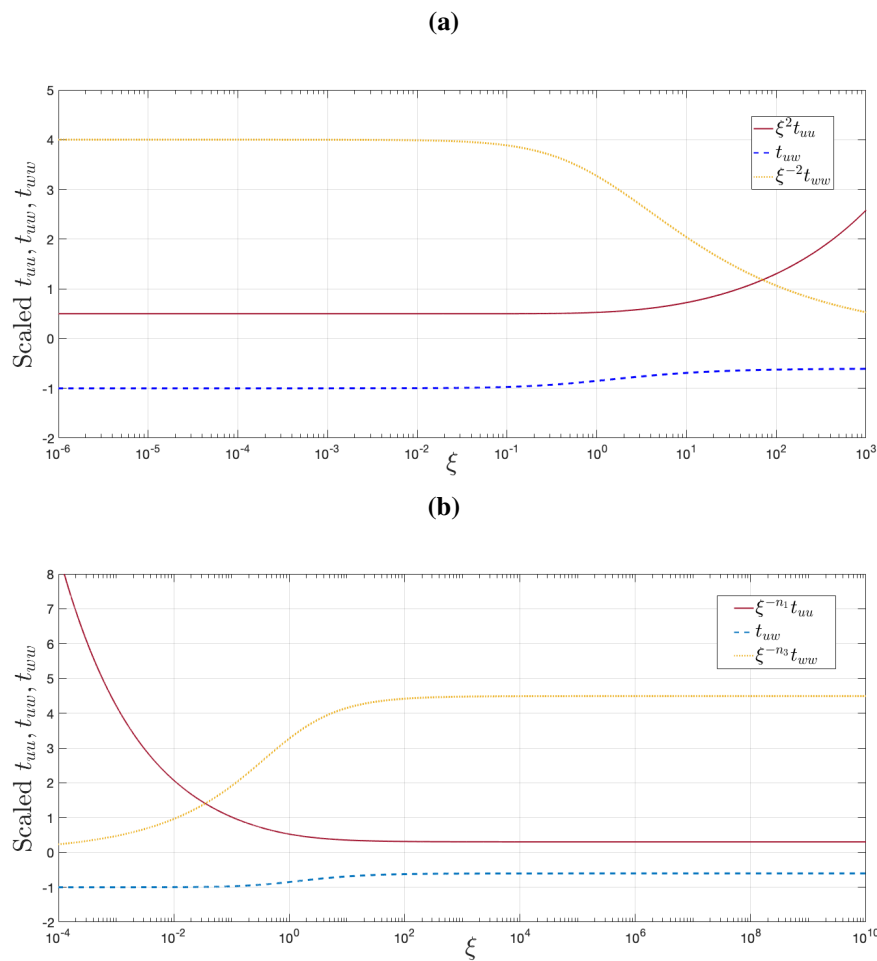
Figure 4. Numerical solution to (3.31)–(3.33) as an initial value problem for separation angle $\alpha = 7\pi/6 \approx 210^o$, with (3.34) imposed at $\xi = \xi_0 = 10^{-6}$. (a) shows the scaled stress profiles near the wall, confirming the behavior in (3.34). (b) illustrates convergence to the far-field behavior (3.35).

3.3. The stress boundary layer at the free-surface

To derive the asymptotics at the free-surface, we follow the same approach used at the die-wall and introduce an artificial small parameter ϵ through the scaling $x' = \epsilon \bar{X}$ and consider $\bar{X} = O(1)$. The limiting behavior (3.14) and dominant balance in (2.7), determine the scalings for the other variables as

$$y' = \delta \bar{Y} \quad \psi = \epsilon^{\lambda_0} \delta \bar{\Psi}, \quad u = \epsilon^{\lambda_0} \bar{u} \quad v = \epsilon^{\lambda_0 - 1} \delta \bar{v},$$
$$p = \epsilon^{\lambda_0 - 1} \bar{p}, \quad T_{uu} = \epsilon^{-(\lambda_0 + 1)} \bar{T}_{uu}, \quad T_{uw} = \bar{T}_{uw}, \quad T_{ww} = \epsilon^{(\lambda_0 + 1)} \bar{T}_{ww}, \tag{3.37}$$

where $\delta = \epsilon^{\frac{(1-\lambda_0^2)}{(\lambda_0+3)}+1}$ and we again use bars for the boundary layer (or inner) variables. The leading order polymer natural stress equations are now

$$(\bar{\mathbf{u}} \cdot \bar{\nabla})\bar{T}_{uu} + \kappa \bar{T}_{uu}^2 \bar{u}^2 = 0, \tag{3.38}$$

$$(\bar{\mathbf{u}} \cdot \bar{\nabla})\bar{T}_{uw} + + \kappa \bar{T}_{uu}\bar{T}_{uw}\bar{u}^2 = 0, \tag{3.39}$$

$$(\bar{\mathbf{u}} \cdot \bar{\nabla})\bar{T}_{ww} + \kappa \bar{u}^2 \left(\bar{T}_{uw}^2 - a^2 \right) = 0, \tag{3.40}$$

which we note are similar to the die wall boundary layer equations, although crucially missing the $\nabla \cdot \mathbf{w}$ terms, since these are small near the slip surface. From (3.14), these require the outer matching conditions

$$\bar{Y} \to +\infty, \quad \bar{T}_{uu} \sim \frac{C_1 C_\alpha^{n_1}}{\kappa^2 C_0^2}(-\bar{X})^{\lambda_0 n_1} \bar{Y}^{n_1}, \quad \bar{T}_{uw} \sim C_2, \quad \bar{T}_{ww} \sim \kappa^2 C_0^2 C_3 C_\alpha^{n_3}(-\bar{X})^{\lambda_0 n_3} \bar{Y}^{n_3}. \tag{3.41}$$

Similar to the die-wall boundary layer, it may be verified that the stream function and pressure remain unchanged from the their limiting outer behaviors in (3.14). In $\bar{X} < 0$, $\bar{Y} = O(1)$, we thus have

$$\bar{\Psi} = \kappa C_0 C_\alpha(-\bar{X})^{\lambda_0} \bar{Y}, \qquad \bar{p} = 2\beta\kappa C_0 g_0(\alpha)(-\bar{X})^{\lambda_0-1}. \tag{3.42}$$

For this given stream function, the nonlinear polymer stress equations (3.38)–(3.40) possess an exact solution. It may be compactly written in the following similarity form

$$\xi = C_\alpha \bar{Y}(-\bar{X})^{\frac{(\lambda_0^2-1)}{\lambda_0+3}-1} \tag{3.43}$$

$$\bar{T}_{uu} = \frac{(-\bar{X})^{-(\lambda_0+1)}}{\kappa^2(-C_0)} t_{uu}(\xi) \qquad \bar{T}_{uw} = t_{uw}(\xi) \qquad \bar{T}_{ww} = \kappa^2 C_0(-\bar{X})^{\lambda_0+1} t_{ww}(\xi), \tag{3.44}$$

with

$$
\begin{aligned}
t_{uu}(\xi) &= \left(\frac{C_\alpha}{(\lambda_0 + 1)} + \frac{(-C_0)}{C_1} \xi^{-n_1} \right)^{-1} \\
t_{uw}(\xi) &= \frac{(-C_0)}{C_1} C_2 \xi^{-n_1} t_{uu}, \\
t_{ww}(\xi) &= C_3 C_0 \xi^{n_3} + \frac{C_\alpha}{(1 + \lambda_0)} \left(C_2 t_{uw} - a^2 \right).
\end{aligned}
\tag{3.45}
$$

The constants of integration have been determined by matching to the limiting outer behavior (3.14). On the free-surface the stresses are now bounded, the recovery of the quadratic stress terms in this boundary layer, being able to arrest the stress growth from the outer region.

For comparison with the solvent stresses, we record the Cartesian components of the polymer extra-stresses, namely,

$$T_{11}^p = \epsilon^{\lambda_0-1} \bar{T}_{11}^p, \quad T_{12}^p = \epsilon^{\frac{(\lambda_0-1)(\lambda_0+3)}{2(\lambda_0+2)}} \bar{T}_{12}^p, \quad T_{22}^p = \epsilon^{\frac{\lambda_0-1}{\lambda_0+2}} \bar{T}_{22}^p, \tag{3.46}$$

where

$$\bar{T}_{11}^p = \bar{T}_{uu} \bar{u}^2, \quad \bar{T}_{12}^p = \bar{T}_{uu} \bar{u}\bar{v}, \quad \bar{T}_{22}^p = \bar{T}_{uu} \bar{v}^2, \tag{3.47}$$

are the leading order expressions and follow from (2.5). The Cartesian components of the solvent extra-stresses may be deduced from the stream function as

$$T_{11}^s = \epsilon^{\lambda_0-1} \bar{T}_{11}^s, \quad T_{12}^s = \delta\epsilon^{\lambda_0-2} \bar{T}_{12}^s, \quad T_{22}^s = \epsilon^{\lambda_0-1} \bar{T}_{22}^s,$$

with

$$\bar{T}_{11}^s = -\bar{T}_{22}^s = -2\lambda_0 \kappa C_0 C_\alpha(-\bar{X})^{\lambda_0-1}. \tag{3.48}$$

However, the solvent shear stress vanishes for the stream function (3.42) and its scaling has to be determined from the correction term to the stream function in the outer region, which can be shown to be of size $O(\delta^3 \epsilon^{\lambda_0-2})$. Solving for the next term of the stream function provides for unnecessary details and we suffice with recording the scalings for the total extra-stresses in this region as

$$T_{11} = \epsilon^{\lambda_0-1}\left(\beta\bar{T}_{11}^s + (1-\beta)\bar{T}_{11}^p\right),$$

$$T_{12} = \epsilon^{\frac{2(\lambda_0-1)}{(\lambda_0+3)}}(\beta\bar{T}_{12}^s + (1-\beta)\bar{T}_{12}^p),$$

$$T_{22} = \epsilon^{\lambda_0-1}(\beta\bar{T}_{22}^s + \epsilon^{\frac{2(1-\lambda_0^2)}{(\lambda_0+3)}}(1-\beta)\bar{T}_{22}^p). \tag{3.49}$$

Only the polymer normal extra-stress T_{22}^p is subdominant to its solvent counterpart. On the free surface $\bar{Y} = 0$, we obtain elongational behavior for the polymer stress in the form

$$\bar{T}_{11}^p = \frac{(1+\lambda_0)}{\kappa\lambda_0}\dot{e}, \quad \bar{T}_{12}^p = 0, \quad \bar{T}_{22}^p = 0, \tag{3.50}$$

where $\dot{e} = \frac{\partial u_0}{\partial \bar{X}}$ is the elongational rate.

We may now determine the shape of the free-surface using the normal stress condition in (2.4). Introducing the scaled free-surface $h(x') = \epsilon^{\lambda_0+1}H(\bar{X})$, and using the pressure (3.42) and normal total extra-stress (3.49), both evaluated on $y' = \bar{Y} = 0$, the normal stress condition gives

$$\frac{d^2H}{d\bar{X}^2} \sim k(-\bar{X})^{\lambda_0-1}, \quad k = 2\beta\kappa C_a(-C_0)(g_0(\alpha) - \lambda_0 C_\alpha),$$

where $g_0(\alpha) = 1/\sin((1-\lambda_0)\alpha)$ and C_α as given in (3.15). Integrating then gives the position of the free-surface as

$$H(\bar{X}) = \frac{k}{\lambda_0(1+\lambda_0)}(-\bar{X})^{\lambda_0+1},$$

or equivalently

$$h(x') \sim \frac{k}{\lambda_0(1+\lambda_0)}(-x')^{\lambda_0+1}, \tag{3.51}$$

for small negative x'. We note that the constant k vanishes in the "stick-slip" planar flow case $\alpha = 180^o, \lambda_0 = 0.5$ and may be verified to be positive for larger separation angles of interest up until $\alpha = 270^o$. The main conclusion is that it is the solvent stress and pressure that determine the shape of the free-surface at the die exit for the Giesekus model, rather than the polymer stress. As such, the curvature of the free-surface (3.51) is that expected of Newtonian flow and its form is consistent with that conjectured in [38] and discussed in [67]. The singularity is solvent dominated and influences the free-surface through the angle of separation, which is determined by the global flow dynamics within the channel.

4. Numerical simulation results

We present here further comparisons between the numerical results of the full extradute-swell problem and the theoretical asymptotic behaviors. Initial comparisons were made in [49] for parameter values of $Wi = 1, \beta = 0.5$, indicating that the postulated asymtptoics are borne out in the numerical

computations. Here we give comparisons for higher Weissenberg numbers, which not only give larger swelling ratios but supports the persistence of the singularity over greater parameter values.

For the numerical simulation of planar extrusion, we use the volume of fluid method in the rheoTool toolbox [68] of OpenFOAM. Details of the scheme are given in [69] and we use the same implementation specifics (mesh details and solver tolerances for convergence) as given in [49]. The natural stress formulation of the Giesekus constitutive equations were used, rather than rheoTool's default Cartesian stresses. This gave more stable results and allowed attainment of higher Weissenberg numbers. We focus on the parameter case $\beta = 0.5$, with two values of the mobility factor $\kappa = 0.1$ and 0.25 and the selected Weissenberg numbers in the range 1 to 10. The Reynolds number is fixed at 10^{-2} and all results are in the absence of surface tension. The separation angle is estimated as the angle of the tangent to the free-surface at the die wall contact point. Its values are recorded in Table 2, along with the consequent Newtonian eigenvalue calculated from (3.4). Also recorded are the final and maximum extrudate-swell ratios D_{extr}/h and D_{max}/h_0 respectively. The difference in these values illustrate the secondary shrinkage of the extrudate after its initial swell, which is more pronounced with increasing Weissenberg number and smaller mobility factor (the Oldroyd-B model being obtained as κ vanishes). Further, these swell ratios appear consistent with the rheotool M3 values reported in [69] for Weissenberg numbers up to 6 (the upper limit of their results). Figures 5 and 6 show the radial behaviors of the velocity components, pressure and natural stresses along three fixed angles (as orientated in Figure 2) in the parameter cases Wi $= 5, \beta = 0.5$ and $\kappa = 0.25$ or 0.1. The velocities and natural stresses converge to their theoretical behaviors along all three rays, confirming the assumption leading to (3.2) that the velocity field is Newtonian-like near the singularity. The rapid convergence of the natural stresses is noteworthy. The pressure converges notably slower and is clearly affected whether the ray to the contact point is inside or outside the channel. For comparison with Figure 6, in Figure 7 we include the equivalent plots for larger Weissenberg number Wi $= 10$ with $\beta = 0.5, \kappa = 0.1$. Similar trends and rate of convergences are observed, confirming the theoretical asymptotics at this higher Weissenberg number.

Table 2. Extrudate swell ratio, separation and corresponding lead eigenvalue.

| | Wi | $\beta = 1/2$ | | | |
		α	λ_0	D_{extr}/h_0	D_{max}/h_0
	1	3.3590	0.4399	1.1831	1.1837
	2	3.4434	0.4211	1.2377	1.2392
$\kappa = 0.1$	5	3.5622	0.3986	1.3554	1.3889
	7	3.5961	0.3930	1.3841	1.4639
	10	3.6223	0.3889	1.4536	1.5530
	1	3.3305	0.4468	1.1599	1.1604
	2	3.3875	0.4333	1.1831	1.1845
$\kappa = 0.25$	5	3.4609	0.4175	1.2495	1.2716
	7	3.4812	0.4135	1.2638	1.3170
	10	3.4969	0.4104	1.2835	1.3497
Newtonian		3.3386	0.4448	1.1811	1.1820
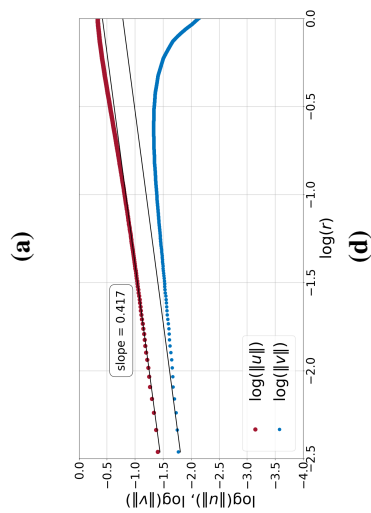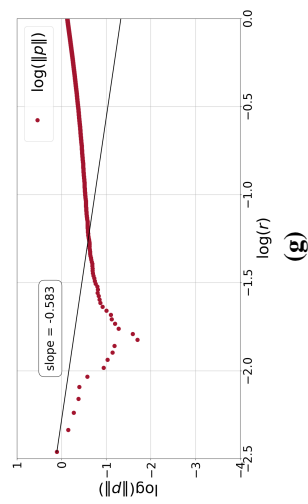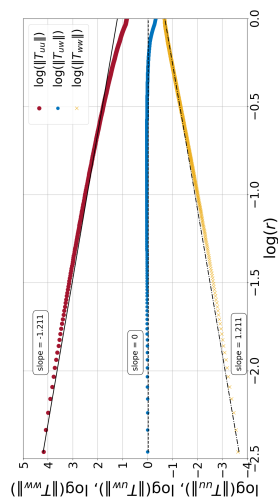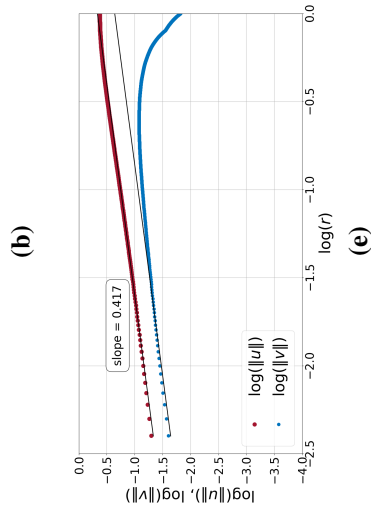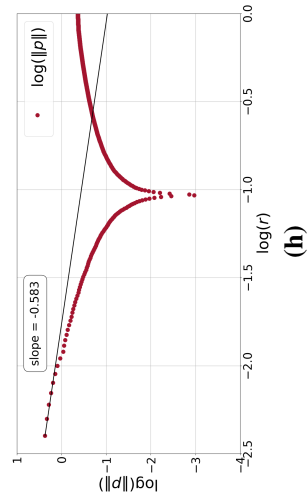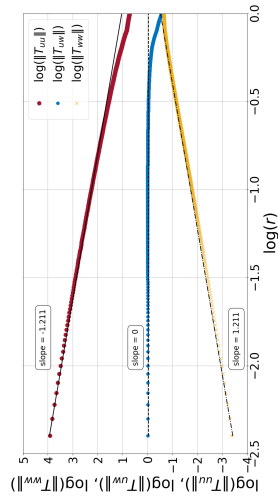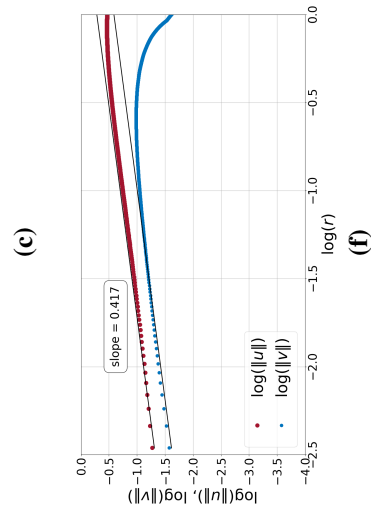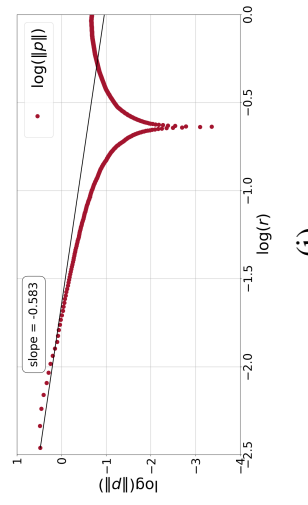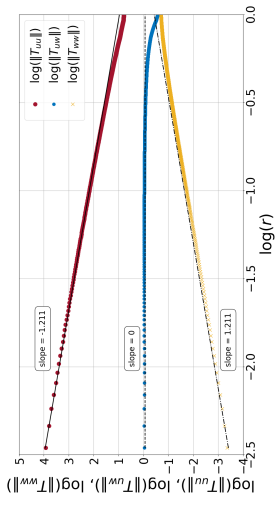
Figure 5. Limiting behavior of (a)–(c) velocity components u and v, (d)–(f) pressure p, and (g)–(i) natural stress components T_{uu}^p, T_{uv}^p, and T_{vv}^p. The left column presents the results along the line $\theta = \frac{\pi}{3}$, the middle column $\theta = \frac{\pi}{2}$, and the right co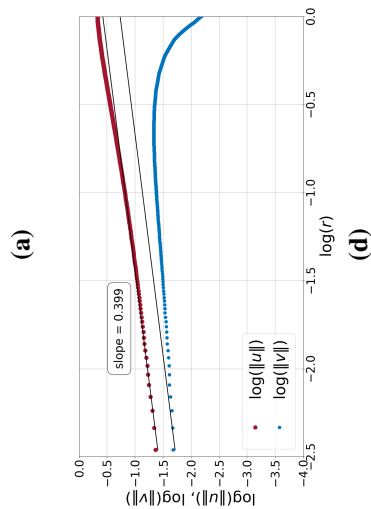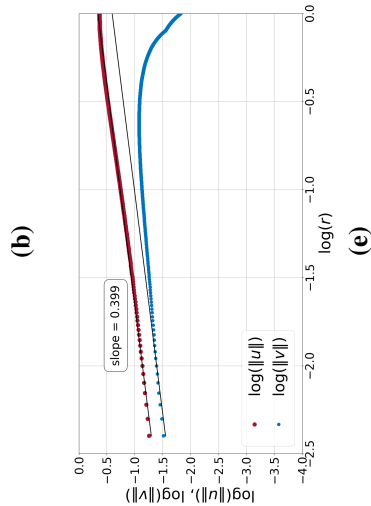lumn $\theta = \frac{2\pi}{3}$. The plotted resu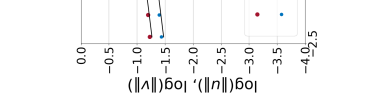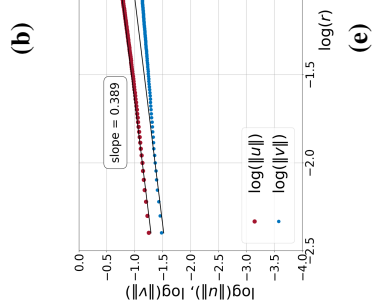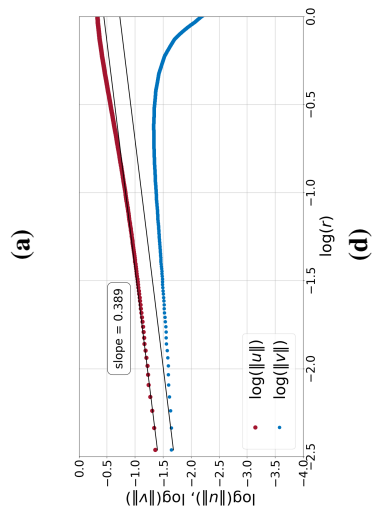lts are for the Giesekus model solved in a natural stress formulation with parameters, Wi $= 5$, $\beta = 0.5$, and $\kappa = 0.25$. Gradient lines: $\lambda_0 \approx 0.418$, $-(1-\lambda_0) \approx -0.582$, $(1+\lambda_0)n_1 \approx -1.211$, $(1+\lambda_0)n_2 = 0$, $(1+\lambda_0)n_3 \approx 1.211$.
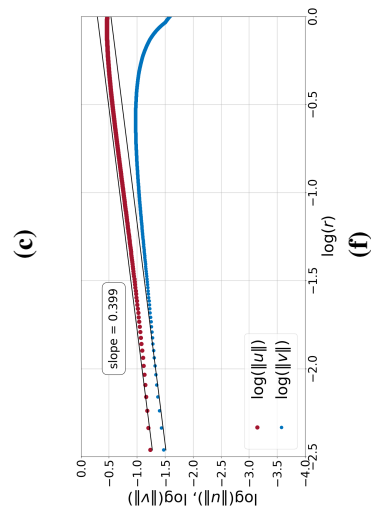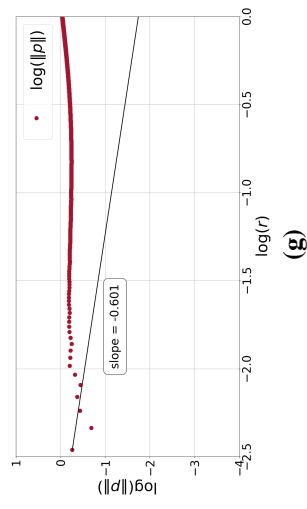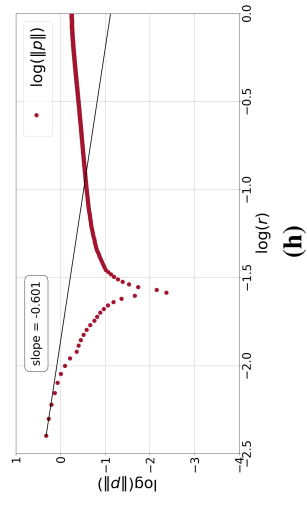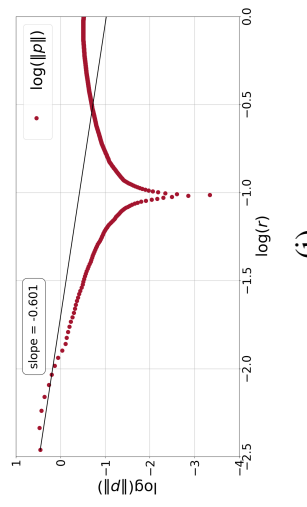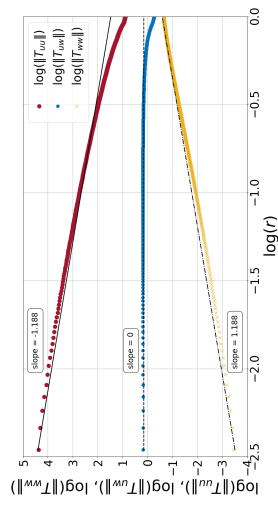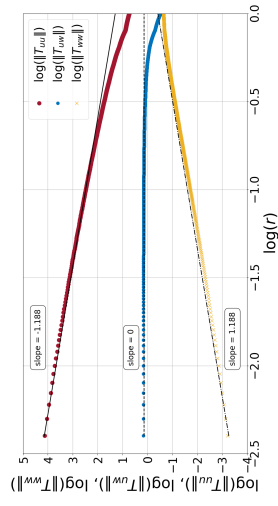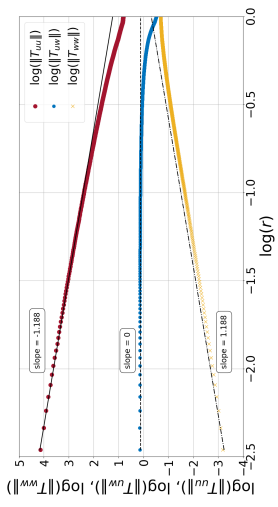
Figure 6. Limiting behavior of (a)–(c) velocity components u_x and u_y, (d)–(f) pressure p, and (g)–(i) natural stress components T_{uu}^p, T_{uw}^p, and T_{ww}^p. The left column presents the results along the line $\theta = \frac{\pi}{2}$, the middle column $\theta = \frac{\pi}{3}$, and the right column $\theta = \frac{2\pi}{3}$. The results are for the Giesekus model solved in a natural stress formulation with parameters, Wi $= 5$, $\beta = 0.5$, and $\kappa = 0.1$. Gradient lines: $\lambda_0 \approx 0.399$, $-(1 - \lambda_0) \approx -0.601$, $(1 + \lambda_0)n_1 \approx -1.188$, $(1 + \lambda_0)n_2 = 0$, $(1 + \lambda_0)n_3 \approx 1.188$.
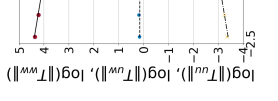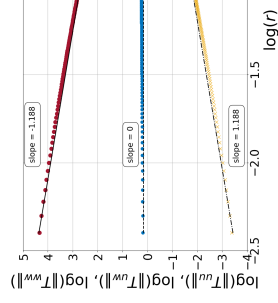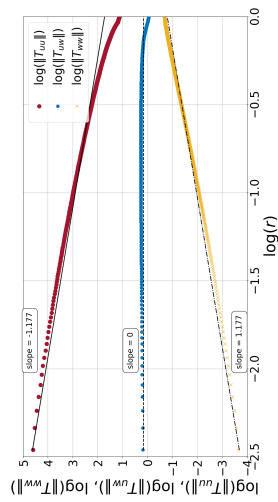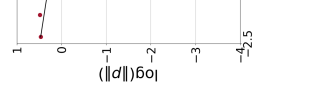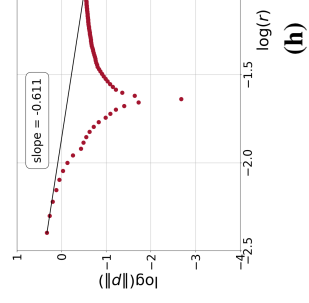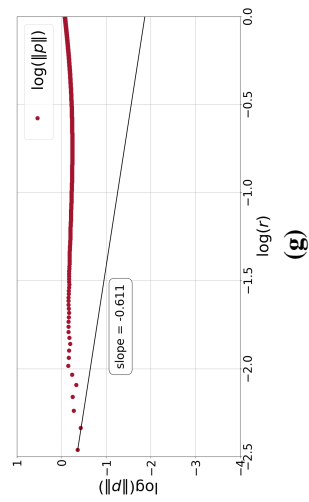
Figure 7. Limiting behavior of (a)–(c) velocity components u_x and u_y, (d)–(f) pressure p, and (g)–(i) natural stress components T_{uu}^p, T_{uw}^p, and T_{ww}^p. The left column presents the results along the line $\theta = \frac{\pi}{3}$, the middle column $\theta = \frac{\pi}{2}$, and the right column $\theta = \frac{2\pi}{3}$. The results plotted correspond to the Giesekus model solved in a natural stress formulation with parameters, $Wi = 10$, $\beta = 0.5$, and $\kappa = 0.1$. Gradient lines: $\lambda_0 \approx 0.389$, $-(1-\lambda_0) \approx -0.611$, $(1+\lambda_0)n_1 \approx -1.177$, $(1+\lambda_0)n_2 = 0$, $(1+\lambda_0)n_3 \approx 1.177$.

5. Conclusions

The details of the matched asymptotic expansion approach for the contact line singularity occurring in extrude swell have been provided here for the Giesekus model. Similar to the simplified PTT model [49, 51], the solvent stress dominates the polymer stress, except in boundary layers at both the die wall and the free-surface. The solution has been detailed here for these narrow regions. In both boundary layers, the polymer and solvent stresses are comparable and are required for the polymer stress to adjust either to the no-slip condition on the die wall or the zero shear stress on the free-surface.

We may compare the boundary layer thicknesses at the die wall and free-surface. These are given by the y scaling in (3.17) and y' scaling in (3.37), which we denote as

$$\delta_{wall} = \epsilon^{\frac{3-\lambda_0}{2}}, \qquad \delta_{jet} = \epsilon^{\frac{(1-\lambda_0^2)}{(\lambda_0+3)}+1}.$$

The free-surface boundary layer is thicker than that at the die wall for $\lambda_0 < 1$, correponding to all separation angles greater than 129°. This should be contrasted to the sPTT model where the free-surface boundary becomes thinner than that at the die wall for separation angles greater than 199.2^o. The narrowest values of the boundary layers occurs when $\lambda_0 = 1/3$ corresponds to the 270° angle of separation, when we have

$$\delta_{wall} \approx \epsilon^{1.33}, \qquad \delta_{jet} \approx \epsilon^{1.27}. \tag{5.1}$$

These are smaller than the corresponding values in the sPTT case [51].

We have demonstrated the validity of the main asymptotic result (3.9) through its comparison with full numerical simulations of the problem in Section 4. As such, we may use this comparison to now estimate the length scales on which the asymptotics emerge. Figures 5–7 suggest the estimate $\epsilon = 10^{-2}$ as an approximate upper bound on the distance on which the singularity asymptotics and numerical solution agree. We note that this value is limited by the velocity and solvent stresses, the convergence of the polymer stresses being on larger length scales that increase with the Weissenberg number (the polymer results in [49] indicate $\epsilon = 10^{-2}$ for Wi$= 1$ whilst here in Figure 7 it extends up to $\epsilon = 10^{-0.5}$ for Wi$=10$). On the length scale at which the solvent singularity emerges around 10^{-2}, the narrowest boundary layer thickness using (5.1) is $\delta_{wall} \approx 2 \times 10^{-3}$. Numerical grids far finer than this would be required to adequately resolve the boundary layers. This shows the extent of the challenges in performing accurate numerical simulations for these models.

The analysis has also elucidated the influence of the stress singularity on the free-surface. The shape of the free-surface local to the singularity is given by (3.51), which shows that it is primarily influenced by the Newtonian eigenvalue. Thus it is the solvent stress rather than the polymer stress that determines the curvature of the surface. However, the polymer stress does play a role in determining the separation angle of the surface, attributed to the relaxation of the normal polymer stresses [19]. It is this influence that allows the Giesekus model to attain far higher swelling ratios than Newtonian fluids due to its larger separation angles.

The asymptotic structure presented here, is valid for the wide parameter ranges $\beta \in (0, 1]$ and $\kappa > 0$. However, if either the solvent viscosity vanishes, $\beta = 0$, or the mobility factor vanishes, $\kappa = 0$, then the nature of the singularity changes. These cases require separate consideration and results are currently outstanding. In the polymer melt case $\beta = 0$, the Newtonian velocity field is lost and a decoupling of the velocity and pressure fields from the polymer stress no longer occurs. Simulation results have been

obtained for this case in extrudate swell [70], although no investigation on the nature of the singularity has been undertaken. When the mobility factor vanishes, we obtain the Oldroyd-B model for which the solvent stress no longer dominates the polymer stress. Whether this model is well-posed in this geometry is an outstanding issue, due to its unbounded stresses at finite strain rates in elongational flow [12]. Notwithstanding these isolated parameter cases, the asymptotic results presented here are expected to hold for all positive Weissenberg numbers.

Author contributions

J. D. Evans: Conceptualization, writing-original draft preparation, formal analysis, software, reviewing and editing; M. L. Evans: Formal analysis and software. All authors have read and approved the final version of the manuscript for publication.

Acknowledgments

Conflict of interest

The authors declare no conflicts of interest.

References

1. G. C. Georgiou, L. G. Olson, W. W. Schultz, S. Sagan, A singular finite element for stokes flow: The stick-slip problem, *Int. J. Numer. Meth. Fl.*, **9** (1989), 1353–1367. https://doi.org/10.1002/fld.1650091105

2. G. C. Georgiou, W. W. Schultz, L. G. Olson, Singular finite elements for the sudden-expansion and the die-swell problems, *Int. J. Numer. Meth. Fl.*, **10** (1990), 357–372. https://doi.org/10.1002/fld.1650100402

3. M. Elliotis, G. Georgiou, C. Xenophontos, Solution of the planar Newtonian stick-slip problem with the singular function boundary integral method, *Int. J. Numer. Meth. Fl.*, **48** (2005), 1001–1021. https://doi.org/10.1002/fld.973

4. R. I. Tanner, A theory of die-swell, *J. Polym. Sci. Pol. Phys.*, **8** (1970), 2067–2078. https://doi.org/10.1002/pol.1970.160081203

5. R. Tanner, A theory of die-swell revisited, *J. Non-Newton. Fluid*, **129** (2005), 85–87. https://doi.org/10.1016/j.jnnfm.2005.05.010

6. R. Tanner, X. Huang, Stress singularities in non-Newtonian stick-slip and edge flows, *J. Non-Newton. Fluid*, **50** (1993), 135–160.

7. S. Rosenblat, Rivulet flow of a viscoelastic liquid, *J. Non-Newton. Fluid*, **13** (1983), 259–277. https://doi.org/10.1016/0377-0257(83)80024-X

8. A. J. Tanasijczuk, C. A. Perazzo, J. Gratton, Navier-Stokes solutions for steady parallel-sided pendent rivulets, *Eur. J. Mech. B-Fluid.*, **29** (2010), 465–471. https://doi.org/10.1016/j.euromechflu.2010.06.002

9. F. H. H. A. Mukahal, B. R. Duffy, S. K. Wilson, Rivulet flow of generalized newtonian fluids, *Phys. Rev. Fluids*, **3** (2018), 083302.

10. J. Vlachopoulos, D. Strutt, Polymer processing, *Mater. Sci. Technol.*, **19** (2003), 1161–1169. https://doi.org/10.1179/026708303225004738

11. E. Mitsoulis, Computational polymer processing, *Model. Simul. Poly.*, **4** (2010), 127–195. https://doi.org/10.1007/s00502-010-0743-0

12. R. Bird, R. C. Armstrong, O. Hassager, *Dynamics of polymeric liquids*, Nashville, TN: John Wiley & Sons, 2 Eds., **1** (1987).

13. C. W. Macosko, *Rheology: Principles, measurements, and applications*, Wiley, 1994.

14. J. M. Dealy, K. F. Wissbrun, *Melt rheology and its role in plastics processing*, Kluwer Academic, 1999.

15. R. Larson, P. S. Desai, Modeling the rheology of polymer melts and solutions, *Ann. Rev. Fluid Mech.*, **47** (2015), 47–65. https://doi.org/10.1146/annurev-fluid-010814-014612

16. M. Denn, Extrusion instabilities and wall slip, *Annu. Rev. Fluid Mech.*, **33** (2001), 265–287. https://doi.org/10.1002/ar.1053

17. R. G. Larson, Instabilities in viscoelastic flows, *Rheol. Acta*, **31** (1992), 213–263. https://doi.org/10.1007/BF00366504

18. D. Tang, F. H. Marchesini, L. Cardon, D. R. D'hooge, State of the-art for extrudate swell of molten polymers: From fundamental understanding at molecular scale toward optimal die design at final product scale, *Macromol. Mater. Eng.*, **305** (2020), 2000340. https://doi.org/10.1002/mame.202000340

19. S. Richardson, The die swell phenomenon, *Rheologica Acta*, **9** (1970), 193–199. https://doi.org/10.1007/BF01973479

20. O. Hassager, Working group on numerical techniques, *J. Non-Newton. Fluid*, **29** (1988), 2–5.

21. S. Middleman, J. Gavis, Expansion and contraction of capillary jets of viscoelastic liquids, *Phys. Fluids*, **4** (1961), 963–969. https://doi.org/10.1063/1.1706446

22. J. Gavis, S. Middleman, Origins of normal stress in capillary jets of Newtonian and viscoelastic liquids, *J. Appl. Polym. Sci.*, **7** (1963), 493–506. https://doi.org/10.1002/app.1963.070070208

23. W. W. Graessley, S. D. Glasscock, R. L. Crawley, Die swell in molten polymers, *T. Soc. Rheol.*, **14** (1970), 519–544.

24. L. A. Utracki, Z. Bakerdjian, M. R. Kamal, A method for the measurement of the true die swell of polymer melts, *J. Appl. Polym. Sci.*, **19** (1975), 481–501. https://doi.org/10.1002/app.1975.070190213

25. D. C. Huang, J. L. White, Extrudate swell from slit and capillary dies: An experimental and theoretical study, *Polym. Eng. Sci.*, **19** (1979), 609–616. https://doi.org/10.1002/pen.760190904

26. S. Middleman, J. Gavis, Expansion and contraction of capillary jets of Newtonian liquids, *Phys. Fluids*, **4** (1961), 355–359. https://doi.org/10.1063/1.1706332

27. S. L. Goren, S. Wronski, The shape of low-speed capillary jets of Newtonian liquids, *J. Fluid Mech.*, **25** (1966), 185–198. https://doi.org/10.1017/S0022112066000120

28. J. Batchelor, J. Berry, F. Horsfall, Die swell in elastic and viscous fluids, *Polymer*, **14** (1973), 297–299. https://doi.org/10.1016/0032-3861(73)90121-3

29. R. E. Nickell, R. I. Tanner, B. Caswell, The solution of viscous incompressible jet and free-surface flows using finite-element methods, *J. Fluid Mech.*, **65** (1974), 189–206. https://doi.org/10.1017/S0022112074001339

30. R. L. Gear, M. Keentok, J. F. Milthorpe, R. I. Tanner, The shape of low Reynolds number jets, *Phys. Fluids*, **26** (1983), 7–9. https://doi.org/10.1063/1.863987

31. E. B. Dussan, On the spreading of liquids on solid surfaces: Static and dynamic contact lines, *Ann. Rev. Fluid Mech.*, **11** (1979), 371–400. https://doi.org/10.1146/annurev.fl.11.010179.002103

32. C. Huh, L. E. Scriven, Hydrodynamic model of steady movement of a solid/liquid/fluid contact line, *J. Colloid Interf. Sci.*, **35** (1971), 85–101. https://doi.org/10.1016/0021-9797(71)90188-3

33. G. J. Jameson, M. C. G. del Cerro, Theory for the equilibrium contact angle between a gas, a liquid and a solid, *J. Chem. Soc.*, **72** (1976), 883–895. https://doi.org/10.1039/f19767200883

34. G. J. Merchant, J. B. Keller, Contact angles, *Phys. Fluids A Fluid Dynam.*, **4** (1992), 477–485. https://doi.org/10.1063/1.858320

35. J. C. Slattery, E. Oh, K. Fu, Extension of continuum mechanics to the nanoscale, *Chem. Eng. Sci.*, **59** (2004), 4621–4635. https://doi.org/10.1016/j.ces.2004.06.046

36. M. E. Diaz, M. D. Savage, R. L. Cerro, The effect of temperature on contact angles and wetting transitions for n-alkanes on PTFE, *J. Colloid Interf. Sci.*, **503** (2017), 159–167. https://doi.org/10.1016/j.jcis.2017.05.003

37. W. J. Silliman, L. E. Scriven, Separating how near a static contact line: Slip at a wall and shape of a free surface, *J. Comput. Phys.*, **34** (1980), 287–313. https://doi.org/10.1016/0021-9991(80)90091-1

38. W. W. Schultz, C. Gervasio, A study of the singularity in the die-swell problem, *Q. J. Mech. Appl. Math.*, **43** (1990), 407–425. https://doi.org/10.1093/qjmam/43.3.407

39. T. R. Salamon, D. E. Bornside, R. C. Armstrong, R. A. Brown, The role of surface tension in the dominant balance in the die swell singularity, *Phys. Fluids*, **7** (1995), 2328–2344. https://doi.org/10.1063/1.868746

40. T. R. Salamon, D. E. Bornside, R. C. Armstrong, R. A. Brown, Local similarity solutions in the presence of a slip boundary condition, *Phys. Fluids*, **9** (1997), 1235–1247. https://doi.org/10.1063/1.869263

41. Y. Kulkarni, T. Fullana, S. Zaleski, Stream function solutions for some contact line boundary conditions: Navier slip, super slip and the generalized Navier boundary condition, *P. Roy. Soc. A Math. Phys. Eng. Sci.*, **479** (2023). https://doi.org/10.1098/rspa.2023.0141

42. T. R. Salamon, D. E. Bornside, R. C. Armstrong, R. A. Brown, Local similarity solutions for the stress field of an Oldroyd-b fluid in the partial-slip/slip flow, *Phys. Fluids*, **9** (1997), 2191–2209. https://doi.org/10.1063/1.869342

43. L. M. Hocking, A moving fluid interface on a rough surface, *J. Fluid Mech.*, **76** (1976), 801–817. https://doi.org/10.1017/S0022112076000906

44. R. G. Larson, *Constitutive equations for polymer melts and solutions*, Butterworth-Heinemann, 1988.

45. H. Giesekus, A simple constitutive equation for polymer fluids based on the concept of deformation-dependent tensorial mobility, *J. Non-Newton. Fluid*, **11** (1982), 69–109. https://doi.org/10.1016/0377-0257(82)85016-7

46. H. Giesekus, Stressing behaviour in simple shear flow as predicted by a new constitutive model for polymer fluids, *J. Non-Newton. Fluid*, **12** (1983), 367–374. https://doi.org/10.1016/0377-0257(83)85009-5

47. A. Beris, R. Armstrong, R. Brown, Finite element calculation of viscoelastic flow in a journal bearing: II. moderate eccentricity, *J. Non-Newton. Fluid*, **19** (1986), 323–347. https://doi.org/10.1016/0377-0257(86)80055-6

48. H. K. Moffatt, Viscous and resistive eddies near a sharp corner, *J. Fluid Mech.*, **18** (1964), 1–18. https://doi.org/10.1017/S0022112064000015

49. J. D. Evans, M. L. Evans, The extrudate swell singularity of Phan-Thien-Tanner and Giesekus fluids, *Phys. Fluids*, **31** (2019), 113102. https://doi.org/10.1063/1.5129664

50. J. Evans, Stick-slip singularity of the giesekus fluid, *J. Non-Newton. Fluid*, **222** (2015), 24–33. https://doi.org/10.1016/j.jnnfm.2014.08.012

51. J. D. Evans, M. L. Evans, Stress boundary layers for the Phan-Thien-Tanner fluid at the static contact line in extrudate swell, *J. Eng. Math.*, 2024, in press. https://doi.org/10.21203/rs.3.rs-3934625/v1

52. G. Schleiniger, R. J. Weinacht, A remark on the Giesekus viscoelastic fluid, *J. Rheol.*, **35** (1991), 1157–1170. https://doi.org/10.1122/1.550169

53. L. D. Sturges, Die swell: The separation of the free surface, *J. Non-Newton. Fluid*, **6** (1979), 155–159. https://doi.org/10.1016/0377-0257(79)87012-3

54. M. Renardy, The stresses of an upper convected Maxwell fluid in a Newtonian velocity field near a re-entrant corner, *J. Non-Newton. Fluid*, **50** (1993), 127–134. https://doi.org/10.1016/0377-0257(93)80027-9

55. M. Renardy, How to integrate the upper convected Maxwell (UCM) stresses near a singularity (and maybe elsewhere, too), *J. Non-Newton. Fluid*, **52** (1994), 91–95. https://doi.org/10.1016/0377-0257(94)85060-7

56. M. I. Gerritsma, T. N. Phillips, On the use of characteristic variables in viscoelastic flow problems, *IMA J. Appl. Math.*, **66** (2001), 127–147. https://doi.org/10.1093/imamat/66.2.127

57. M. I. Gerritsma, T. N. Phillips, On the characteristics and compatibility equations for the UCM model fluid, *ZAMM-J. Appl. Math. Mech./ZAMM*, **88** (2008), 523–539. https://doi.org/10.1002/zamm.200700058

58. R. G. Owens, T. N. Phillips, *Computational rheology*, Imperial College Press, 2002.

59. M. L. Evans, *The extrudate swell singularity of viscoelastic fluids*, PhD thesis, University of Bath, 2020.

60. M. Renardy, The high Weissenberg number limit of the UCM model and the Euler equations, *J. Non-Newton. Fluid*, **69** (1997), 293–301. https://doi.org/10.1016/S0377-0257(96)01544-3

61. T. Hagen, M. Renardy, Boundary layer analysis of the Phan-Thien-Tanner and Giesekus model in high Weissenberg number flow, *J. Non-Newton. Fluid*, **73** (1997), 181–189. https://doi.org/10.1016/S0377-0257(97)00035-9

62. P. Lagerstrom, J. Cole, Examples illustrating expansion procedures for the Navier-Stokes equations, *Indiana Univ. Math. J.*, **4** (1955), 817–882. https://doi.org/10.1512/iumj.1955.4.54032

63. I. Chang, Navier-stokes solutions at large distances from a finite body, *J. Math. Mech.*, **10** (1961), 811–876. https://doi.org/10.1512/iumj.1961.10.10055

64. M. V. Dyke, *Perturbation methods in fluid mechanics*, Academic Press, New York and London, 1964.

65. P. A. Lagerstrom, *Matched asymptotic expansions*, Springer, New York, 1988.

66. J. Kevorkian, J. D. Cole, *Perturbation methods in applied mathematics*, Springer, New York, 1981.

67. R. G. Owens, The separation angle of the free surface of a viscous fluid at a straight edge, *J. Fluid Mech.*, **942** (2022). https://doi.org/10.1017/jfm.2022.408

68. F. Pimenta, M. A. Alves, *RheoTool*, 2016. Available from: `https://github.com/fppimenta/rheoTool`.

69. R. Comminal, F. Pimenta, J. H. Hattel, M. A. Alves, J. Spangenberg, Numerical simulation of the planar extrudate swell of pseudoplastic and viscoelastic fluids with the streamfunction and the VOF methods, *J. Non-Newton. Fluid*, **252** (2108), 1–18. https://doi.org/10.1016/j.jnnfm.2017.12.005

70. M. Tomé, M. Araujo, J. Evans, S. McKee, Numerical solution of the Giesekus model for incompressible free surface flows without solvent viscosity, *J. Non-Newton. Fluid*, **263** (2109), 104–119. https://doi.org/10.1016/j.jnnfm.2018.11.007